Bond Order Solid of Two-Dimensional Dipolar Fermions

S. G. Bhongale,[1] L. Mathey,[2,3] Shan-Wen Tsai,[4] Charles W. Clark,[3] and Erhai Zhao[1]

[1]*School of Physics, Astronomy and Computational Sciences, George Mason University, Fairfax, Virginia 22030, USA*
[2]*Zentrum für Optische Quantentechnologien and Institut für Laserphysik, Universität Hamburg, 22761 Hamburg, Germany*
[3]*Joint Quantum Institute, National Institute of Standards and Technology & University of Maryland, Gaithersburg, Maryland 20899, USA*
[4]*Department of Physics and Astronomy, University of California, Riverside, California 92521, USA*

(Received 9 December 2011; published 2 April 2012)

The recent experimental realization of dipolar Fermi gases near or below quantum degeneracy provides an opportunity to engineer Hubbard-like models with long-range interactions. Motivated by these experiments, we chart out the theoretical phase diagram of interacting dipolar fermions on the square lattice at zero temperature and half filling. We show that, in addition to p-wave superfluid and charge density wave order, two new and exotic types of bond order emerge generically in dipolar fermion systems. These phases feature homogeneous density but periodic modulations of the kinetic hopping energy between nearest or next-nearest neighbors. Similar, but manifestly different, phases of two-dimensional correlated electrons have previously only been hypothesized and termed ''density waves of nonzero angular momentum.'' Our results suggest that these phases can be constructed flexibly with dipolar fermions, using currently available experimental techniques.

DOI: 10.1103/PhysRevLett.108.145301 PACS numbers: 67.85.−d, 67.80.−s, 71.10.Fd

The experimental demonstration of Bose-Einstein condensation of atomic chromium [1] and dysprosium [2], both of which have large magnetic dipole moments, ushers the ultracold dipolar gas to the arena of quantum emulation [3,4]. A gas of the fermionic isotope of dysprosium, ^{161}Dy, has been cooled below quantum degeneracy [5]. A high space-density gas of ^{40}K^{87}Rb, fermionic molecules with electric dipole moments, has recently been produced near quantum degeneracy [6] and confined in optical lattice [7]. Such systems are expected to show a rich array of quantum phases arising from the long-range and anisotropic nature of dipole-dipole interaction [8–10]. This uniquely distinguishes the dipolar Fermi gas from other Fermi systems, e.g., the 2D electron gas, the quantum fluid of ^{3}He, and Fermi gases of alkali atoms with short-range interactions. Previous works on dipolar Fermi gases have investigated the anisotropic Fermi liquid properties [10,11], the pairing instability [12–16], phases showing density modulation [17,18], as well as liquid crystal states [19–21]. The possibility of supersolid phases [22] has also been discussed.

For a 2D dipolar Fermi gas on a square lattice at half filling, with dipole moments perpendicular to the plane, one expects to find a checkerboard density modulation, known as the charge density wave (CDW; we follow the nomenclature even though atoms or molecules are charge neutral). When the dipole moments are aligned in the lattice plane, the system becomes an anisotropic superfluid and the attractive interaction binds fermions into Cooper pairs. The main question we address here is, how do different orders compete or cooperate as the dipole moments are turned from perpendicular to parallel orientation?

We employ the functional renormalization group (FRG) technique [23–25], along with the self-consistent mean field (SCMF) [26], to obtain, for the first time, the zero-temperature phase diagram of dipolar fermions on a two-dimensional square lattice at half filling. The FRG takes an unbiased approach to treat *all* the instabilities of the Fermi surface, revealing the existence of two new and fascinating quantum phases: the p-wave bond order solid (BOS$_p$) and the d-wave bond order solid (BOS$_d$). These bond order solids may be considered as 2D analogues of the ''bond order wave'' found in the 1D extended Hubbard model [27–29].

We model single-component dipolar fermions on a two-dimensional square lattice with lattice constant a_L by the Hamiltonian

$$H = -t\sum_{\langle ij\rangle} a_i^\dagger a_j + \frac{1}{2}\sum_{i\neq j} V_{ij} n_i n_j, \tag{1}$$

where t represents the nearest-neighbor hopping, a_i is the fermion annihilation operator at the site i, and $n_i = a_i^\dagger a_i$ is the number operator. The site index i represents a lattice site centered at $\mathbf{r}_i = i_x a_L \hat{x} + i_y a_L \hat{y}$, where i_x and i_y are integers. The matrix elements of the dipole interaction in the two-particle Wannier basis are given by $V_{ij} = \langle ij|V_{dd}|ij\rangle = V_d[1 - 3(\hat{r}_{ij}\cdot\hat{d})^2]/(r_{ij}/a_L)^3$, where $\mathbf{r}_{ij} \equiv \mathbf{r}_i - \mathbf{r}_j$ and the dipoles are pointing in the same direction $\hat{d}$. We assume an external electric or magnetic field $\mathbf{F}$ pointing in some general direction. Then, the interaction energy of the dipole moment $\mathbf{d}$ with the field $\mathbf{F}$ is equal to $-\mathbf{F}\cdot\mathbf{d}$, implying that the orientation of the dipole moments can be tuned by $\mathbf{F}$. We label the direction of $\mathbf{d}$

by polar and azimuthal angles θ_F and ϕ_F, respectively, as illustrated in the schematic of Fig. 1(a).

The interaction between dipoles can be attractive or repulsive, depending on θ_F, ϕ_F, and $\mathbf{r}_{ij}$. For example [refer to Fig. 1(a)], if $\phi_F = 0$, $V_y \equiv V_{dd}(a_L\hat{y})$ is always repulsive, while $V_x \equiv V_{dd}(a_L\hat{x})$ and $V_3 \equiv V_{dd}(a_L\hat{x} + a_L\hat{y})$ become negative for $\theta_F > \vartheta_{c1} \approx 35.26°$ and $\theta_F > \vartheta_{c2} = \cos^{-1}(1/\sqrt{3}) \approx 54.74°$, respectively. We shall show that these two critical points, ϑ_{c1} and ϑ_{c2}, roughly set the phase boundary between the checkerboard charge density wave (cb-CDW), the BOS$_p$, and the Bardeen-Cooper-Schrieffer (BCS) superfluid phase, for the $\phi_F = 0$ case.

We now discuss the $T = 0$ phase diagram at half filling. First, we analyze the weakly interacting limit, $V_d < t$, using the FRG. In this approach, no assumptions about possible dominant orders are necessary. Rather, the method includes all processes near the Fermi surface of the noninteracting system via the generalized four-point vertex function: $U_\ell(\mathbf{k}_1, \mathbf{k}_2, \mathbf{k}_3)$, where $\mathbf{k}_{1,2}$ ($\mathbf{k}_{3,4}$) are incoming (outgoing) momenta and $\mathbf{k}_4 = \mathbf{k}_1 + \mathbf{k}_2 - \mathbf{k}_3$. Here, ℓ is the renormalization group flow parameter that relates the energy cutoff Λ to the initial cutoff Λ_0 (chosen to be $4t$) via $\Lambda_\ell = \Lambda_0 e^{-\ell}$. Starting with the bare vertex U_0, progressively tracing out the high energy degrees of freedom, a set of coupled integro-differential equations gives the FRG flow for all the vertices.

The renormalized vertices for specific channels of interest, e.g.,

$$U_\ell^{\mathrm{NEST}}(\mathbf{k}_1, \mathbf{k}_2) = U_\ell(\mathbf{k}_1, \mathbf{k}_2, \mathbf{k}_1 + \mathbf{Q}),$$
$$U_\ell^{\mathrm{BCS}}(\mathbf{k}_1, \mathbf{k}_2) = U_\ell(\mathbf{k}_1, -\mathbf{k}_1, \mathbf{k}_2), \quad (2)$$

are extracted by appropriately constraining the incoming and outgoing momenta. Here, $\mathbf{Q} = (\pi, \pm\pi)$ is the nesting vector at half filling for the square lattice and U_ℓ^{NEST} is the same as U_ℓ^{CDW} of Ref. [24]. The channel matrix with the largest divergent eigenvalue λ corresponds to the most dominant instability of the Fermi liquid. The corresponding eigenvector ψ, defined on the Fermi surface, indicates the symmetry of the incipient order parameter associated with the instability.

We perform the FRG analysis for a range of values of V_d, θ_F, and ϕ_F, producing a 3D phase diagram, visualized in Fig. 1(b) as slice cuts along two different planes. To capture and emphasize the key elements of the phase diagram, first we fix $\phi_F = 0$, generating a 2D phase diagram in the θ_F-V_d plane shown in the left panel of Fig. 1(b). Next, we fix $V_d = 0.5t$ instead, yielding the θ_F-ϕ_F plane shown in the right panel of Fig. 1(b).

The θ_F-V_d phase diagram shows the existence of three phases separated by two critical angles $\theta_F = \theta_1$ and θ_2, with no appreciable dependence on V_d. For $0 \le \theta_F < \theta_1$, the nesting channel has the largest (most divergent) eigenvalue λ. The corresponding eigenvector ψ_{NEST}, as illustrated in the top panel of Fig. 2(a), is almost constant, with only small modulation along the Fermi surface. This implies the onset of CDW order with s-wave symmetry, identified as a checkerboard modulation of on-site density—the cb-CDW shown in Fig. 1(e). The physical origin of this phase can be traced by observing that $\theta_1 \approx \vartheta_{c1}$; thus, V_x, V_y, $V_3 > 0$ in this regime, allowing for a low-energy configuration with density concentrated on the next-to-nearest-neighbor sites, consistent with the perfect nesting of the Fermi surface. For $\theta_2 \le \theta_F \le 90°$, the BCS channel exhibiting a p-wave symmetry is the most diverging under the FRG flow [see Fig. 2(a)]. In real space, this corresponds to the onset of nearest-neighbor pairing, $\langle a_i a_{i+\hat{x}}\rangle = -\langle a_i a_{i-\hat{x}}\rangle$, generated by couplings V_x and V_3, both becoming attractive for $\theta_F > \theta_2 \sim \vartheta_{c2}$. The

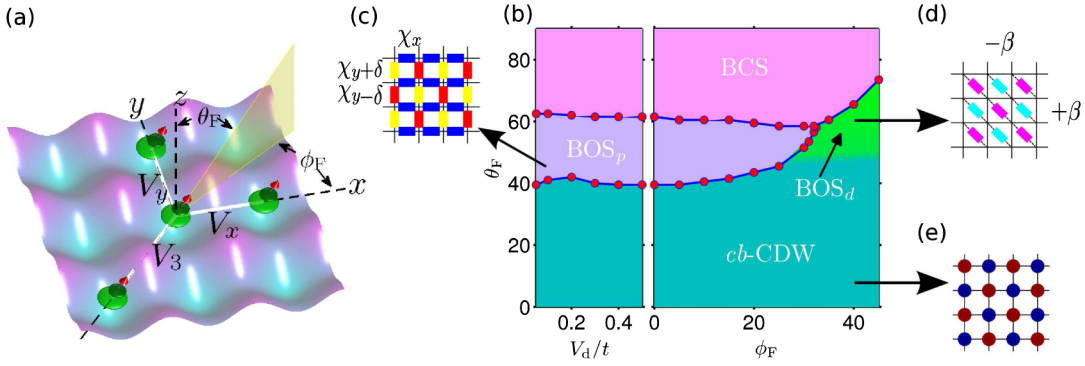

FIG. 1 (color online). Dipolar fermions on square lattice. (a) Schematic of the dipolar fermions confined to a square optical lattice potential. The induced dipole moment $\mathbf{d}$ points along the direction $\hat{d} = \cos\theta_F\hat{z} + \sin\theta_F\cos\phi_F\hat{x} + \sin\theta_F\sin\phi_F\hat{y}$. (b) Phase diagram obtained via the FRG indicating four phases: p-wave bond order solid (BOS$_p$), d-wave bond order solid (BOS$_d$), checkerboard charge density wave (cb-CDW), and p-wave BCS superfluid (BCS). Left: phase diagram in the θ_F-V_d plane at $\phi_F = 0$. Right: phase diagram in the θ_F-ϕ_F plane at $V_d = 0.5t$. The phase boundary (solid line) is determined by the abrupt change in the symmetry of the eigenvector of the dominant instability (see Fig. 2). The smooth crossover from the cb-CDW and the BOS$_d$ is indicated by a gradual change of the color shading. (c)–(e) Schematics of the bond or density modulation pattern for the BOS$_p$, BOS$_d$, and cb-CDW phases, respectively.

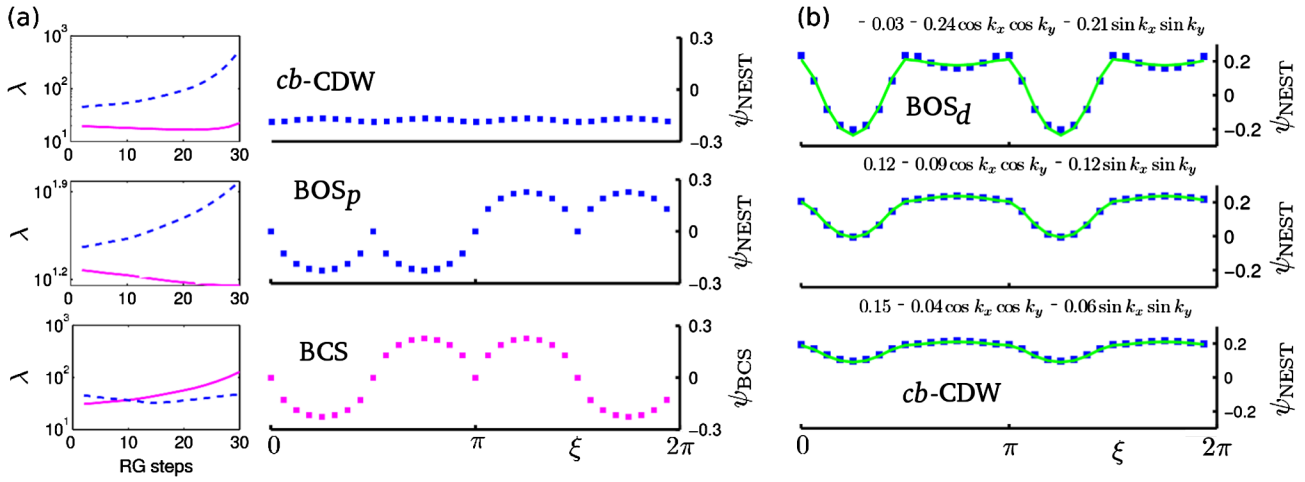

FIG. 2 (color online). FRG results for $V_d = 0.5t$. The FRG is implemented numerically by discretizing the Fermi surface into 32 patches distributed at equally spaced angular points. (a) Top, middle, and bottom panels represent the FRG results for $(\theta_F, \phi_F) = (30°, 0)$, $(42°, 0)$, and $(70°, 0)$, respectively. Left column: the largest eigenvalues λ of the NEST (dashed line) and BCS (solid line) channels. Right column: the corresponding eigenvector ψ of the most diverging channel as a function of ξ, the angular position on the Fermi surface defined by $\tan\xi = k_y/k_x$, plotted with square markers. (b) Top, middle, and bottom panels represent the FRG results for $(\theta_F, \phi_F) = (62°, 40°)$, $(46°, 40°)$, and $(38°, 40°)$, plotted using square markers. The fit is shown in the solid line. As θ_F is increased, ψ smoothly changes from nodeless for $\theta_F \lessapprox 46°$ to one with nodes for $\theta_F \gtrapprox 46°$.

superfluid phase here is the lattice analog of the p-wave BCS phase discussed previously for continuum dipolar Fermi gases [8,14,16].

Finally, the intermediate regime, $\theta_1 \leq \theta_F < \theta_2$, is the most intriguing. The FRG predicts a leading instability in the nesting channel, similar to the cb-CDW, but instead with a p-wave symmetry, $\psi_{\rm NEST}(\mathbf{k}) \sim \chi(\mathbf{k}) = \chi_0 \sin k_y$, as shown in the middle panel of Fig. 2(a). This result suggests a broken symmetry phase, shown in Fig. 1(c), with periodic modulation of $\langle a_i^\dagger a_{i+\hat{y}} - \chi_y\rangle = -\langle a_i^\dagger a_{i-\hat{y}} - \chi_y\rangle = \delta(-1)^{i_x+i_y}$, where χ_y is the average of $\langle a_i^\dagger a_{i+\hat{y}}\rangle$ over all bonds. We observe that the nesting vector $\mathbf{Q}$ is consistent with the checkerboard pattern of the bond variable representing nearest-neighbor hopping. We refer to this broken symmetry phase as the p-wave bond order solid (BOS$_p$). Phases with similar, but manifestly different, bond order patterns were conjectured by Nayak and referred to as p-density waves [30].

The right panel of Fig. 1(b), the θ_F-ϕ_F phase diagram at fixed interaction strength $V_d = 0.5t$, shows the three phases above for small values of ϕ_F. However, as ϕ_F is increased towards 45°, the BOS$_p$ region shrinks and eventually disappears beyond $\phi_F \sim 35°$. Such a change is due to the new features in the dipolar interactions for ϕ_F close to 45°, where $V_x \sim V_y$, but the next-to-nearest-neighbor interactions along $\hat{x} + \hat{y}$ and $\hat{x} - \hat{y}$ develop opposite signs. We find that, for such large values of $\phi_F \sim 45°$, the eigenvector can be fit very well by $\psi_{\rm NEST}(\mathbf{k}) = \alpha + \beta[\cos k_x \cos k_y + \sin k_x \sin k_y]$, as seen in the right panel of Fig. 2(b). As θ_F is increased, the constant term α, which describes the density modulation of cb-CDW order, is gradually reduced, while the magnitude of β increases. In the light shaded region labeled by BOS$_d$ in Fig. 1(b), α/β drops gradually from 1 to 0 as θ_F is increased toward the phase boundary to BCS. We refer to this region where the $\cos k_x \cos k_y$ and $\sin k_x \sin k_y$ components of $\psi_{\rm NEST}$ are dominant as the d-wave bond order solid (BOS$_d$). In this phase, the density and the nearest hopping $\langle a_i^\dagger a_{i+\hat{x}/\hat{y}}\rangle$ are homogeneous. However, the dipolar interaction induces an effective diagonal hopping, $\langle a_i^\dagger a_{i-\hat{x}+\hat{y}}\rangle$, a bond variable with amplitude proportional to β, and a spatial pattern shown schematically in Fig. 1(d). The BOS$_d$ found here differs from the d_{xy} density wave conjectured in Ref. [30].

To firmly pin down the nature of the phases, we complement the FRG analysis with the SCMF theory (see Ref. [26]) on a square lattice of finite size $L \times L$ with a periodic boundary condition by defining the normal and pair density matrices $\rho_{ij} = \langle a_j^\dagger a_i\rangle$ and $m_{ij} = \langle a_i a_j\rangle$, respectively. The corresponding mean fields are then given by $\chi_{ji} = -\sum_{kl}\langle jk|V_{dd}|li\rangle\rho_{lk}$ and $\Delta_{ij} = -\frac{1}{2}\sum_{kl}\langle ij|V_{dd}|kl\rangle m_{lk}$. The dipole interaction is retained up to a distance of $10a_L$. We search for the ground state iteratively by starting with an initial guess for $\boldsymbol{\rho}$ and $\boldsymbol{m}$, until desired convergence is reached. The phase boundaries are obtained by comparing the thermodynamic potential for various converged solutions (see the Supplemental Material [31]). The chemical potential is tuned to maintain half filling, and the lattice size $L > 20a_L$ is varied to check that the results do not depend on the choice of L.

The SCMF phase diagram for $\phi_F = 0$, shown in Fig. 3, confirms the existence and interpretation of the three

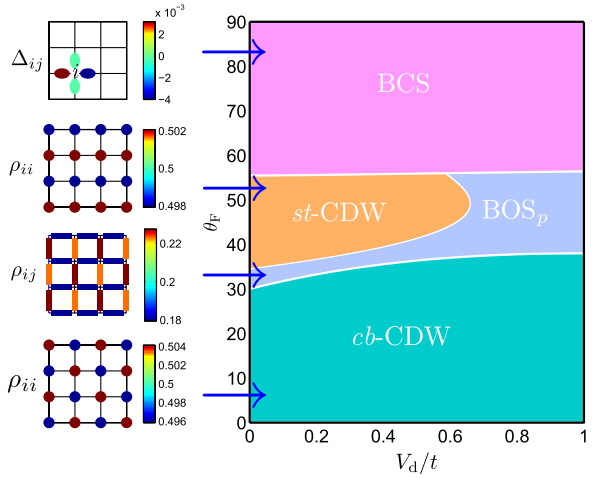

FIG. 3 (color online). SCMF phase diagram. Shown on the left are representatives of the on-site density ρ_{ii}, the nearest-neighbor hopping ρ_{ij} (with $j = i + \hat{x}$ or $j = i + \hat{y}$), or the pairing gap Δ_{ij}, corresponding to the four phases at $V_d = 0.5t$. The lattice size is 32×32.

phases found in the FRG analysis. The phase boundaries are in qualitative agreement with those from the FRG. The SCMF for nonzero ϕ_F also identifies the BOS$_d$ as a phase with the bond modulation pattern illustrated in Fig. 1(d). We caution that the SCMF phase diagram is only suggestive. For example, the SCMF predicts an additional striped density wave phase, the *st*-CDW, which is not expected to survive at $V_d \ll t$. This illustrates that the SCMF is insufficient to describe competing orders, as opposed to the FRG. The possibility of the *st*-CDW and collapse instability beyond the weak coupling regime is further discussed in Ref. [31].

We now provide some intuitive understanding of the bond order phases by considering a simplified mean field version of Eq. (1), keeping only the nearest-neighbor interactions V_x and V_y. The mean field decoupling of the interaction term gives $-n_i n_j \sim a_i^\dagger a_j a_j^\dagger a_i \to \rho_{ij} a_j^\dagger a_i +$ H.c. $- |\rho_{ij}|^2$. The modulation of the bond variable, $\rho_{ij} = \langle a_i^\dagger a_j \rangle$, in the BOS$_p$ phase at $\phi_F = 0$, has the form shown in Fig. 1(c): $\rho_{i,i\pm\hat{x}} = \chi_x$, $\rho_{i,i\pm\hat{y}} = \chi_y \pm \delta$. The mean field Hamiltonian can be written as $H_R = -2\sum_{\mathbf{k}} \chi_{\mathbf{k}} b_{\mathbf{k}}^\dagger a_{\mathbf{k}} +$ H.c., up to a constant term. Here, $a_{\mathbf{k}}$ and $b_{\mathbf{k}}$ are fermion annihilation operators defined separately on two sublattices related by the lattice translation vector $a_L\hat{x}$, and $\chi_{\mathbf{k}} = (t + V_x\chi_x)\cos k_x + (t + V_y\chi_y)\cos k_y - iV_y\delta \sin k_y$. The ground-state energy per unit cell is then given by $E_{\mathrm{GS}} = -2(\chi_x + \chi_y)(t + V_x + V_y) - 2V_y\delta^2$, clearly indicating that finite bond modulation δ is energetically favored for positive V_y. The $\phi_F = 90°$ situation is identical, only with the x and y axes interchanged, and hence a 90° rotated bond pattern. Thus, the BOS$_d$ phase, with a checkerboard pattern of next-to-nearest bonds near $\phi_F = 45°$, naturally connects the two BOS$_p$ phases on either side.

The bond modulation δ, the energy gap, and the transition temperature T_c of the BOS$_p$ phase increase with V_d for weak coupling. Exact diagonalization of Eq. (1) on a 2×8 and 4×4 cluster with periodic boundary conditions shows that the optimal place to observe the BOS$_p$ is at intermediate interaction and tilt angle, e.g., $V_d \sim 2.5t$ and $(\theta_F, \phi_F) = (45°, 0°)$, where the energy gap, and thus T_c, is maximal. Mean field theory estimates an optimal $T_c \sim 0.23t$, or about $0.05E_F$ for half filling, which is not too far from the temperature achieved in the Dy experiment, $T \sim 0.25E_F$ [5]. The BOS$_d$, on the other hand, is most stable in the vicinity of $\phi_F = 45°$ for $\theta_F \sim 60°$. The characteristic density modulation of the *cb*-CDW and *st*-CDW phases uniquely distinguishes them from the other phases and may be detected via *in situ* density imaging. The BCS phase can be detected via pair correlation measurements using noise spectroscopy [32]. Finally, the BOS$_d$ phase may be distinguished from BOS$_p$ by probing the *d*-wave symmetry via the pump-probe scheme discussed in Ref. [33]. Finally, in the presence of a trap potential, the insulating plateau at half filling will be surrounded by metallic regions. The approaches outlined here can be employed to study dipolar Fermi gas away from half filling.

S. B. and E. Z. are supported by NIST Grant No. 70NANB7H6138 Am 001 and ONR Grant No. N00014-09-1-1025A. L. M. acknowledges support from the Landesexzellenzinitiative Hamburg, which is financed by the Science and Research Foundation Hamburg and supported by the Joachim Herz Stiftung. S. W. T. acknowledges support from the NSF under Grant No. DMR-0847801 and from the UC-Lab FRP under Grant No. 09-LR-05-118602.

[1] A. Griesmaier *et al.*, Phys. Rev. Lett. **94**, 160401 (2005).
[2] M. Lu, N. Q. Burdick, S. H. Youn, and B. L. Lev, Phys. Rev. Lett. **107**, 190401 (2011).
[3] A. Micheli, G. K. Brennen, and P. Zoller, Nature Phys. **2**, 341 (2006).
[4] A. V. Gorshkov *et al.*, Phys. Rev. Lett. **107**, 115301 (2011).
[5] M. Lu, N. Q. Burdick, and B. L. Lev, arXiv:1202.4444.
[6] K.-K. Ni *et al.*, Science **322**, 231 (2008).
[7] A. Chotia *et al.*, Phys. Rev. Lett. **108**, 080405 (2012).
[8] M. A. Baranov, Phys. Rep. **464**, 71 (2008).
[9] T. Lahaye *et al.*, Rep. Prog. Phys. **72**, 126401 (2009).
[10] B. M. Fregoso and E. Fradkin, Phys. Rev. Lett. **103**, 205301 (2009).
[11] C.-K. Chan, C. Wu, W.-C. Lee, and S. Das Sarma, Phys. Rev. A **81**, 023602 (2010).
[12] M. A. Baranov, L. Dobrek, and M. Lewenstein, Phys. Rev. Lett. **92**, 250403 (2004).
[13] M. A. Baranov, M. S. Mar'enko, V. S. Rychkov, and G. V. Shlyapnikov, Phys. Rev. A **66**, 013606 (2002).

[14] G. M. Bruun and E. Taylor, Phys. Rev. Lett. **101**, 245301 (2008).
[15] N. R. Cooper and G. V. Shlyapnikov, Phys. Rev. Lett. **103**, 155302 (2009).
[16] C. Zhao *et al.*, Phys. Rev. A **81**, 063642 (2010).
[17] Y. Yamaguchi, T. Sogo, T. Ito, and T. Miyakawa, Phys. Rev. A **82**, 013643 (2010).
[18] K. Mikelsons and J. K. Freericks, Phys. Rev. A **83**, 043609 (2011).
[19] J. Quintanilla, S. T. Carr, and J. J. Betouras, Phys. Rev. A **79**, 031601(R) (2009).
[20] K. Sun, C. Wu, and S. Das Sarma, Phys. Rev. B **82**, 075105 (2010).
[21] C. Lin, E. Zhao, and W. V. Liu, Phys. Rev. B **81**, 045115 (2010); **83**, 119901(E) (2011).
[22] L. He and W. Hofstetter, Phys. Rev. A **83**, 053629 (2011).
[23] R. Shankar, Rev. Mod. Phys. **66**, 129 (1994).
[24] D. Zanchi and H. J. Schulz, Phys. Rev. B **61**, 13 609 (2000).
[25] L. Mathey, S.-W. Tsai, and A. H. Castro Neto, Phys. Rev. Lett. **97**, 030601 (2006); Phys. Rev. B **75**, 174516 (2007).
[26] J.-P. Blaizot and G. Ripka, *Quantum Theory of Finite Systems* (MIT Press, Cambridge, MA, 1985).
[27] M. Nakamura, Phys. Rev. B **61**, 16 377 (2000).
[28] P. Sengupta, A. W. Sandvik, and D. K. Campbell, Phys. Rev. B **65**, 155113 (2002).
[29] K.-M. Tam, S.-W. Tsai, and D. K. Campbell, Phys. Rev. Lett. **96**, 036408 (2006).
[30] C. Nayak, Phys. Rev. B **62**, 4880 (2000).
[31] See Supplemental Material at http://link.aps.org/supplemental/10.1103/PhysRevLett.108.145301 for a more detailed discussion of the theoretical methods.
[32] E. Altman, E. Demler, and M. D. Lukin, Phys. Rev. A **70**, 013603 (2004).
[33] D. Pekker, R. Sensarma, and E. Demler, arXiv:0906.0931.